Hindawi
International Journal of Electrochemistry
Volume 2023, Article ID 2386013, 10 pages
https://doi.org/10.1155/2023/2386013

Research Article

Effect of Surface Composition on Electrochemical Oxidation Reaction of Carbon Monoxide and Ethanol of Pt_xRh_{1-x} Solid Solution Electrodes

Nguyen Trung Kien, Haruki Yara, Masanobu Chiku, Eiji Higuchi, and Hiroshi Inoue

Department of Applied Chemistry, Graduate School of Engineering, Osaka Metropolitan University, Sakai, Osaka 599-8531, Japan

Correspondence should be addressed to Eiji Higuchi; higuchi@omu.ac.jp

Received 27 July 2023; Revised 2 November 2023; Accepted 6 November 2023; Published 15 November 2023

Academic Editor: Hamish Andrew Miller

Pt_xRh_{1-x} ($x = 0.76$, 0.54, and 0.27) solid solutions were prepared by arc-melting. For these solid solutions, the lattice constant was linearly related to the Pt content. The surface compositions of the solid solutions determined by X-ray photoelectron spectroscopy were quite similar to their bulk compositions estimated by energy dispersive X-ray spectroscopy. The CO-stripping voltammograms demonstrated that the onset potential of CO oxidation current density (E_{onset}) shifted negatively as the surface Pt content decreased, suggesting an increased CO-poisoning resistance. Linear sweep voltammograms of the solid solution electrodes in an Ar-saturated (1 M ethanol + 0.1 M $HClO_4$) solution exhibited that the onset potentials of ethanol oxidation reaction (EOR) current for all solid solution electrodes were lower than of a Pt electrode, and $Pt_{0.54}Rh_{0.46}$ gave the highest specific activity (SA) of 312 $\mu A \cdot cm^{-2}$, which was about 1.8 and 2.5 times higher than the SAs of Pt and Rh, respectively. *In situ* infrared reflection-absorption spectra exhibited that the $Pt_{0.54}Rh_{0.46}$ electrode had the bands due to the linear-bonded CO on Pt and bridge-bonded CO on Rh as EOR intermediates around 0.2 V vs. the reversible hydrogen electrode, but the band due to the linear-bonded CO on Rh was not observed even at 0.6 V, suggesting that the existence of the adjacent Pt-Rh sites and the preferential formation of bridge-bonded CO on Rh accelerated the C-C bond cleavage and improved the EOR activity.

1. Introduction

Ethanol has a high energy density (8.0 $kWh \cdot kg^{-1}$) [1, 2] and can be mass-produced from biofuels generated from plant-based waste materials such as biomass. Thus, direct ethanol fuel cell (DEFC) is attracting attention as carbon-neutral power sources. However, to improve the slow rate of ethanol oxidation reaction (EOR) in DEFC, the research and development of electrocatalysts with high activity and high durability have been performed [3–5]. The CO species as an EOR intermediate is known to poison electrocatalysts, resulting in a significant decrease in EOR catalytic activity [1, 6–8]. In addition, the cleavage reaction of the C-C bond required for the complete EOR to CO_2 is difficult [1, 9–14].

Pt nanoparticle catalysts exhibit excellent EOR activity, but their surfaces are easily poisoned by intermediately-generated CO species. Binary alloys of Pt with foreign metals such as Ru [15, 16], Sn [12, 14, 17–19], and Rh [1, 10, 20–27] exhibit high EOR activity in acidic media. Among them, PtRh alloys had the highest EOR activity [1, 20–23, 26]. Wang et al. evaluated the EOR activity of Pt_xRh_{100-x} ($x = 91$, 76, 52, 24) alloys whose compositions were determined by energy dispersive X-ray spectroscopy (EDX) and found that the $Pt_{76}Rh_{24}$ alloy showed the highest EOR activity [20]. Piwowar et al. reported that the amount of produced CO_2 per electrochemical active surface area (ECSA) of Pt_xRh_{1-x} ($x = 0.71$, 0.51, and 0.36) nanoalloys loaded on carbon black (Pt_xRh_{1-x}/C) at 0.95 V vs. RHE was independent of the surface Rh content [26]. The CO_2 selectivity was also improved for PtRh/C [24] and Pt overlayer on Rh [25]. Zhu et al. reported that PtRh nanowires loaded on carbon black (PtRh NW/C) had significantly high C-C breaking ability to

promote the complete EOR [1]. In addition, they found that the EOR activity and durability of the PtRh NW/C at 1.0 V vs. RHE in (0.1 M $HClO_4$ + 0.5 M C_2H_5OH) aqueous solution evaluated by cyclic voltammetry were nearly three times as high as those of Pt/C, and the faradaic efficiency for CO_2 production in potentiostatic electrolysis at 1.0 V vs. RHE for the former was 57%, which was much higher than that of Pt/C (17%), clearly indicating that the Rh component is effective for improving the CO_2 selectivity [1]. Delpeuch et al. also reported that PtRh nanodendrites had high EOR activity in acidic media, and the EOR activity strongly depended on surface composition, in contrast to the results of Piwowar and Lewera [26].

So far, the EOR activity of PtRh alloy catalysts has been evaluated at potentials over 1.0 V vs. RHE [1, 20–25] that was higher than the potential of oxidative Rh dissolution (0.8 V vs. RHE) [28, 29]. So, the surface composition of PtRh alloys must be changed during the EOR activity evaluation. As a matter of course, the EOR activity evaluation of the PtRh catalysts should be carried out at potentials less than 0.8 V where surface alloy composition is maintained. Meanwhile, for alloy nanoparticles, the surface composition often does not match the bulk composition. Therefore, the surface composition with the highest EOR activity cannot be predicted from the bulk composition. In the present study, Pt_xRh_{1-x} ($x = 0.76$, 0.54, and 0.27) solid solutions whose surface compositions were almost the same as bulk compositions were prepared by an arc-melting method. Their EOR activity in an acidic solution was evaluated at 0.6 V vs. RHE, where Rh does not dissolve oxidatively, and a relationship between surface composition and EOR activity was reevaluated. In addition, the EOR mechanism on the Pt_xRh_{1-x} solid solutions was discussed based on *in situ* infrared reflection-absorption spectra at different potentials.

2. Experimental

2.1. Preparation of Rh and Pt_xRh_{1-x} Solid Solution Electrodes. Ingots (diameter: 3 mm) of Pt, Rh, and Pt_xRh_{1-x} solid solutions with bulk compositions of $x = 0.76$, 0.54, and 0.27 were prepared from constituent elements (99.98% Pt plate and 99.9% Rh wire, Nilaco) by induction melting under an Ar atmosphere. Each solid solution ingot was turned over and remelted four times to ensure homogeneity. The resultant polycrystalline Rh and each Pt_xRh_{1-x} solid solution ingot with a diameter of 3 mm were polished into a hemisphere. The flat side of the hemisphere was used as an electrode, and the other side was connected to a lead wire. The side of the hemisphere was covered with a Teflon tube to prevent contact with an electrolyte solution. On the other hand, a commercial polycrystalline Pt electrode with a diameter of 5 mm (BAS Inc.) was polished with alumina suspensions, followed by sonicating in ultrapure water and ethanol.

2.2. Characterization of Pt, Rh, and Pt_xRh_{1-x} Solid Solution Electrodes. Crystallographic characterization of each ingot was carried out with an X-ray diffractometer (Cu K_α/$\lambda = 1.5405$ Å, 40 kV, 30 mA, XRD-6100, Shimadzu). The bulk composition of each solid solution was determined by EDX (JED-2300, JEOL Ltd.). The evaluation of the electronic state and the determination of surface composition for each solid solution were performed by XPS (ESCA-3400 instrument, Shimazu, Mg K_α radiation 1253.6 eV, 10 kV, and 20 mA). Each XPS spectrum was calibrated using an Au $4f_{7/2}$ peak of gold powder (99.999%, Strem Chemicals) as 84.0 eV.

2.3. Electrochemical Measurements. The polycrystalline Pt electrode has two couples of redox peaks due to hydrogen adsorption/desorption between 0.05 and 0.4 V vs. the reversible hydrogen electrode (RHE) [30, 31]. The electric charge for the desorption of atomic hydrogen ($Q_{\text{H-des}}$) for polycrystalline Pt is 210 μC·cm^{-2} [30], assuming that atomic hydrogen is adsorbed on a Pt atom. The $Q_{\text{H-des}}$ for polycrystalline Rh is 221 μC·cm^{-2} [31]. The redox peaks due to hydrogen desorption for a pure Rh electrode partly overlap with those for the polycrystalline Pt electrode [32, 33]. Rh has a face-centered cubic (fcc) structure, and its atomic radius is similar to that of Pt. So, assuming that Rh has a stoichiometric composition of Rh : H = 1 : 1 like Pt, a $Q_{\text{H-des}}$ value of 210 μC·cm^{-2} was used [31]. The ECSAs of the Pt_xRh_{1-x} electrodes were calculated as follows:

$$\text{ECSA}_{\text{Pt+Rh}} = \frac{Q_{H-\text{des}}}{210}. \quad (1)$$

To evaluate the CO poisoning of the Pt, Rh, and Pt_xRh_{1-x} solid solution surfaces, CO was bubbled through the 0.1 M $HClO_4$ aqueous solution for 5 min with applying a constant potential of 0.30 V vs. RHE. After that, Ar gas was bubbled through the electrolyte solution for approximately 15 min to remove the dissolved CO while keeping the constant potential of 0.30 V. Two cycles of CVs were recorded at 10 mV·s^{-1} between 0.05 and 1.2 V. These operations were performed at 25°C.

CVs and linear sweep voltammograms (LSVs) of each electrode were recorded at 20 mV·s^{-1} in Ar-saturated 0.5 M H_2SO_4 and (1 M ethanol + 0.1 M $HClO_4$) solutions at 30°C, respectively. A platinized Pt electrode and an RHE were used as counter and reference electrodes, respectively.

2.4. Qualitative Analysis of EOR Products and Intermediates. The products and intermediates of EOR were identified by *in situ* IRAS (FT/IR 6100, HgCdTe (MCT) detector, JASCO). The cell is coupled at its bottom with a CaF_2 prism beveled at 60° from the surface normal. The spectra were recorded with a resolution of 4 cm^{-1}. IR spectra were drawn due to the absorbance calculated from reflectance intensities at 0.1–0.6 V (R) and 0.05 V (R^0) for reference.

3. Results and Discussion

3.1. Structure and Compositions of Pt_xRh_{1-x} Solid Solutions. Figure 1(a) shows XRD patterns for $Pt_{0.76}Rh_{0.24}$, $Pt_{0.54}Rh_{0.46}$, and $Pt_{0.27}Rh_{0.73}$ ingots. The diffraction pattern of each Pt_xRh_{1-x} ingot was similar to the diffraction patterns of Pt and Rh with a face-centered cubic (fcc) structure, suggesting that each Pt_xRh_{1-x} ingot also has the fcc structure. All diffraction peaks of these Pt_xRh_{1-x} ingots were located between the

corresponding diffraction peaks of Pt and Rh, as shown in Figure 1. The (111) peak shifted to the higher angles with increasing the Rh content or decreasing the Pt content due to the shrinkage of the unit cell, and the other diffraction peaks also showed the similar tendency. Figure 1(b) shows the lattice constant as a function of the bulk Pt content evaluated by EDX. As can be seen from this figure, the lattice constant linearly increased with the Pt content, suggesting that Vegard's law holds. Thus, the Rh atoms were uniformly incorporated into the Pt crystallites, and binary solid solutions were formed, as expected from the XRD patterns.

Figure 2 shows the Pt4f and Rh3d core-level spectra for Pt, Rh, $Pt_{0.76}Rh_{0.24}$, $Pt_{0.54}Rh_{0.46}$, and $Pt_{0.27}Rh_{0.73}$. The Pt4f spectrum for each solid solution exhibited intense doublets at 71.0 and 74.4 eV, which were assigned to metallic Pt (Pt^0) [1, 27], and there were not any peaks assigned to Pt oxides. On the other hand, the Rh3d spectrum for each solid solution exhibited the $3d_{3/2}$ peak (312.1 eV) and the $3d_{5/2}$ peak (307.3 eV) for Rh^0 [27]. Figure 2 clearly shows that each solid solution had positive shifts of the Pt4f peaks and negative shifts of the Rh3d peaks. The positive and negative peak shifts are related to the downshift and upshift of the d-band center, causing the decrease and increase in the CO adsorption energy [34], respectively, suggesting that the adsorbed CO on Pt is destabilized, whereas that on Rh is stabilized. So, the positive shift of Pt4f peaks for each Pt_xRh_{1-x} solid solution will cause the destabilization of CO adsorbed on the Pt sites.

The surface composition of each Pt_xRh_{1-x} solid solution was determined by XPS, and the relationship between the surface composition and bulk composition for the Pt_xRh_{1-x} solid solutions is shown in Figure 3. As can be seen from Figure 3, the surface Pt content was in good agreement with the bulk Pt content.

3.2. CO Oxidation Behaviors of Pt, Rh, and Pt_xRh_{1-x} Electrodes. To investigate the adsorption/desorption behavior of CO species, CO-stripping voltammograms of the solid solution electrodes were measured. Figures 4(a) and 4(b) show CO-stripping voltammograms of Pt, Rh, $Pt_{0.76}Rh_{0.24}$, $Pt_{0.54}Rh_{0.46}$, and $Pt_{0.27}Rh_{0.73}$ solid solution electrodes. For Pt and Rh electrodes, no hydrogen desorption waves were observed in a potential range of 0.05–0.4 V during the first forward sweep, indicating that the formation of atomic hydrogen on both electrode surfaces was hindered by adsorbed CO. In addition, the CO-stripping current began flowing around 0.62 V for the Rh electrode and 0.74 V for the Pt electrode, suggesting that the adsorbed CO on the Pt surface is more stable than that on the Rh surface. In the second cycle, the CVs of the Pt and Rh electrodes almost agreed with those in an Ar-saturated solution, respectively. Therefore, adsorbed CO on both electrode surfaces was almost removed in the first cycle.

Figure 4(c) shows the onset potential of CO-stripping current ($E_{\text{onset, CO}}$) as a function of surface Pt content. The $E_{\text{onset, CO}}$ was evaluated using a compensated CV that was obtained by subtracting the CV in the 1st cycle from that in the 2nd cycle. As can be seen from Figure 4(c), the $E_{\text{onset, CO}}$ value shifted negatively as the surface Pt content decreased. In a proposed CO oxidation mechanism in the PtRh alloy electrode [20], water is oxidized at the Rh sites to form adsorbed OH (OH_{ad}) (equation (2)), which binds to the adsorbed CO (CO_{ad}) at the adjacent Pt sites (equation (3)).

$$\text{Rh} + \text{H}_2\text{O} \longrightarrow \text{Rh–OH}_{\text{ad}} + \text{H}^+ + \text{e}^-, \quad (2)$$

$$\text{Pt–CO}_{\text{ad}} + \text{Rh–OH}_{\text{ad}} \longrightarrow \text{Pt} + \text{Rh} + \text{CO}_2 + \text{H}^+ + \text{e}^-. \quad (3)$$

Rh, a highly oxophilic transition metal, initiates water dissociation at a lower potential than Pt, as expected from Figure 4(a). The adsorption energy of CO on Pt decreases with the downward shift of the d-band center due to the ligand effect of Rh [1, 34–37], and as expected from Figure 2(a), the d-band center will shift downwardly for each Pt_xRh_{1-x} solid solution. In this way, the ligand effect and bifunctional effect improve the oxidation of adsorbed CO.

Figures 4(d)–4(f) show CVs of $Pt_{0.76}Rh_{0.24}$, $Pt_{0.54}Rh_{0.46}$, and $Pt_{0.27}Rh_{0.73}$ solid solution electrodes in an Ar-saturated 0.1 M $HClO_4$ solution before and after CO-stripping voltammetric measurements. Irrespective of solid solution composition, the hydrogen adsorption/desorption waves did not change after each CO-stripping voltammetric measurement, suggesting that the surface composition of each solid solution did not change during this measurement.

3.3. EOR Activity for the Pt, Rh, and Pt_xRh_{1-x} Electrodes. LSVs of the Pt, Rh, $Pt_{0.76}Rh_{0.24}$, $Pt_{0.54}Rh_{0.46}$, and $Pt_{0.27}Rh_{0.73}$ solid solution electrodes in Ar-saturated (1.0 M C_2H_5OH + 0.1 M $HClO_4$) solution were performed to investigate their EOR activity. The results are shown in Figure 5(a). In addition, the specific activity (SA) of each electrode was evaluated by dividing the EOR current at 0.6 V vs. RHE by $ECSA_{Pt+Rh}$ and shown in Figure 5(b). As can be seen from Figure 5(b), the $Pt_{0.54}Rh_{0.46}$ electrode had the highest SA (312 $\mu A \cdot cm^{-2}$) among the three solid solution electrodes. Figure 5(c) shows the onset potential (E_{onset}) of the EOR current density evaluated from Figure 5(a) as a function of the surface Pt content. The E_{onset} values of the $Pt_{0.76}Rh_{0.24}$, $Pt_{0.54}Rh_{0.46}$, and $Pt_{0.27}Rh_{0.73}$ solid solution electrodes were 0.337, 0.335, and 0.339 V, respectively, each of which was lower than that of Pt (0.342 V). In this way, the Pt_xRh_{1-x} solid solution electrodes improved the EOR activity of Pt and Rh electrodes.

3.4. IRAS Spectra and EOR Mechanism of the Pt, Rh, and Pt_xRh_{1-x} Electrodes. Many EOR mechanisms on Pt electrodes in acidic media have been proposed. In a typical EOR mechanism in acidic media, ethanol molecules are dissociatively adsorbed at the Pt sites with O-adsorption or C-adsorption, and then oxidized to acetaldehyde. Acetaldehyde is dissociatively oxidized to acetyl (CH_3CO_{ad}), which is still oxidized to acetic acid, the final partial oxidation product, by OH_{ad}. In another pathway, it has been proposed that acetaldehyde was dehydrated to form adsorbed enolate, followed by dissociating adsorbed CO and CH_x species through C-C bond cleavage in the potential region of hydrogen desorption [38].

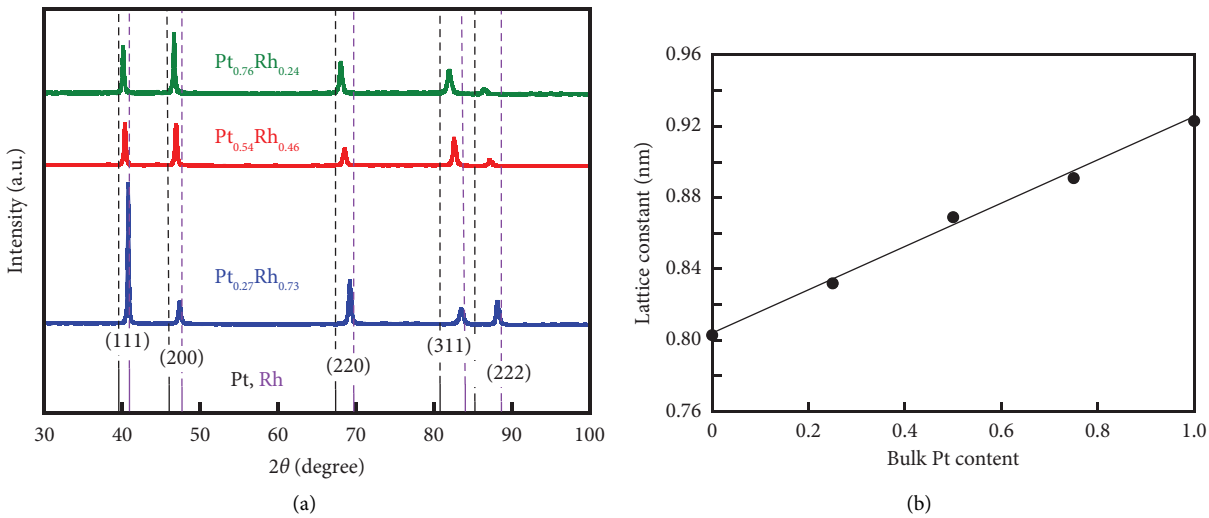

Figure 1: (a) XRD patterns for $Pt_{0.76}Rh_{0.24}$, $Pt_{0.54}Rh_{0.46}$, and $Pt_{0.27}Rh_{0.73}$ solid solutions. (b) The lattice constant as a function of Pt content.

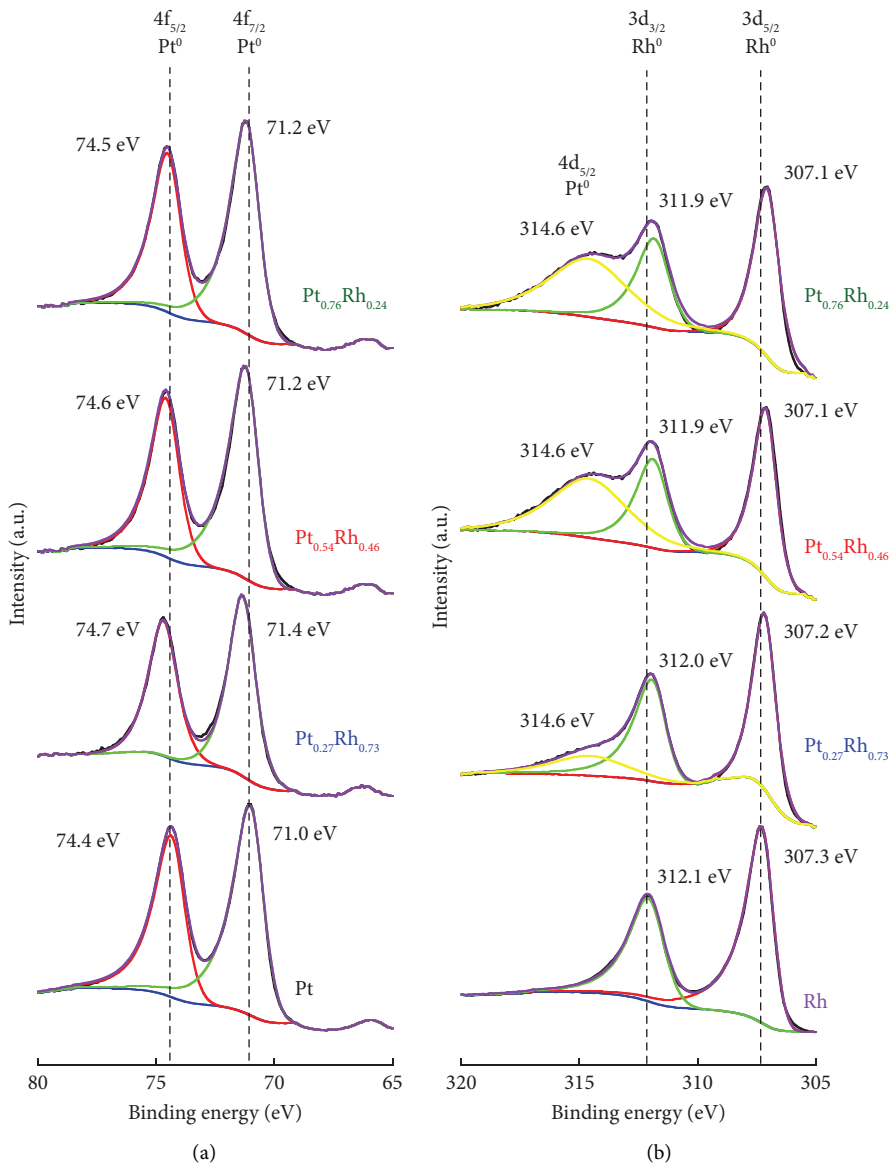

Figure 2: (a) Pt 4f and (b) Rh 3d XPS spectra of Pt, Rh, $Pt_{0.76}Rh_{0.24}$, $Pt_{0.54}Rh_{0.46}$, and $Pt_{0.27}Rh_{0.73}$ solid solutions.

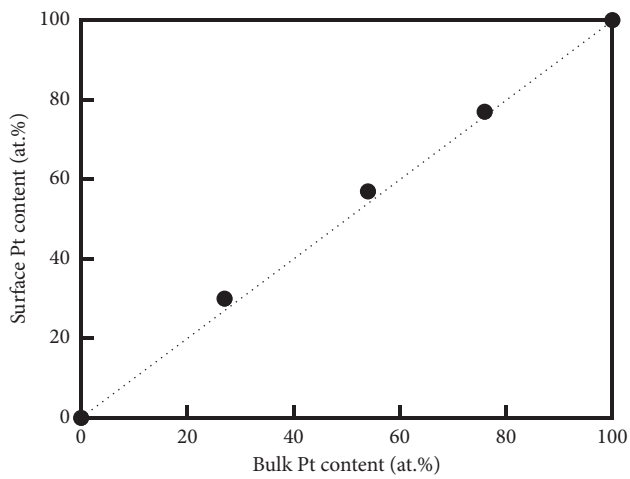

Figure 3: The relationship between surface and bulk compositions for Pt_xRh_{1-x} solid solutions.

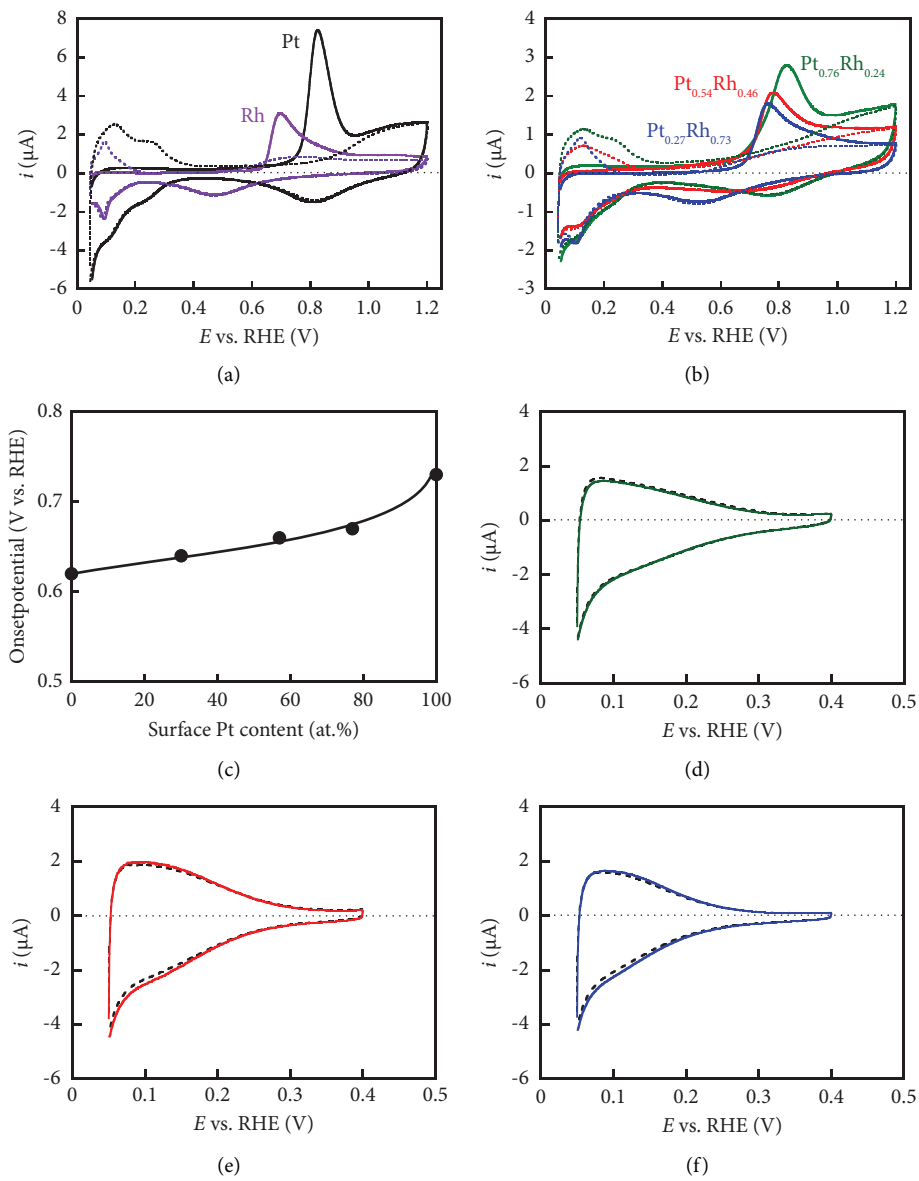

Figure 4: CO stripping voltammograms (solid line: 1st cycle, dashed line: 2nd cycle) of (a) Pt and Rh and (b) $Pt_{0.75}Rh_{0.25}$, $Pt_{0.50}Rh_{0.50}$, and $Pt_{0.25}Rh_{0.75}$ solid solution electrodes. (c) Onset potentials for the CO oxidation reaction as a function of Pt content. Cyclic voltammograms (dashed line: before CO stripping, solid line: after CO stripping) of (d) $Pt_{0.75}Rh_{0.25}$, (e) $Pt_{0.50}Rh_{0.50}$, and (f) $Pt_{0.25}Rh_{0.75}$ solid solution electrodes. Electrolyte: Ar-saturated 0.1 M $HClO_4$ aqueous solution.

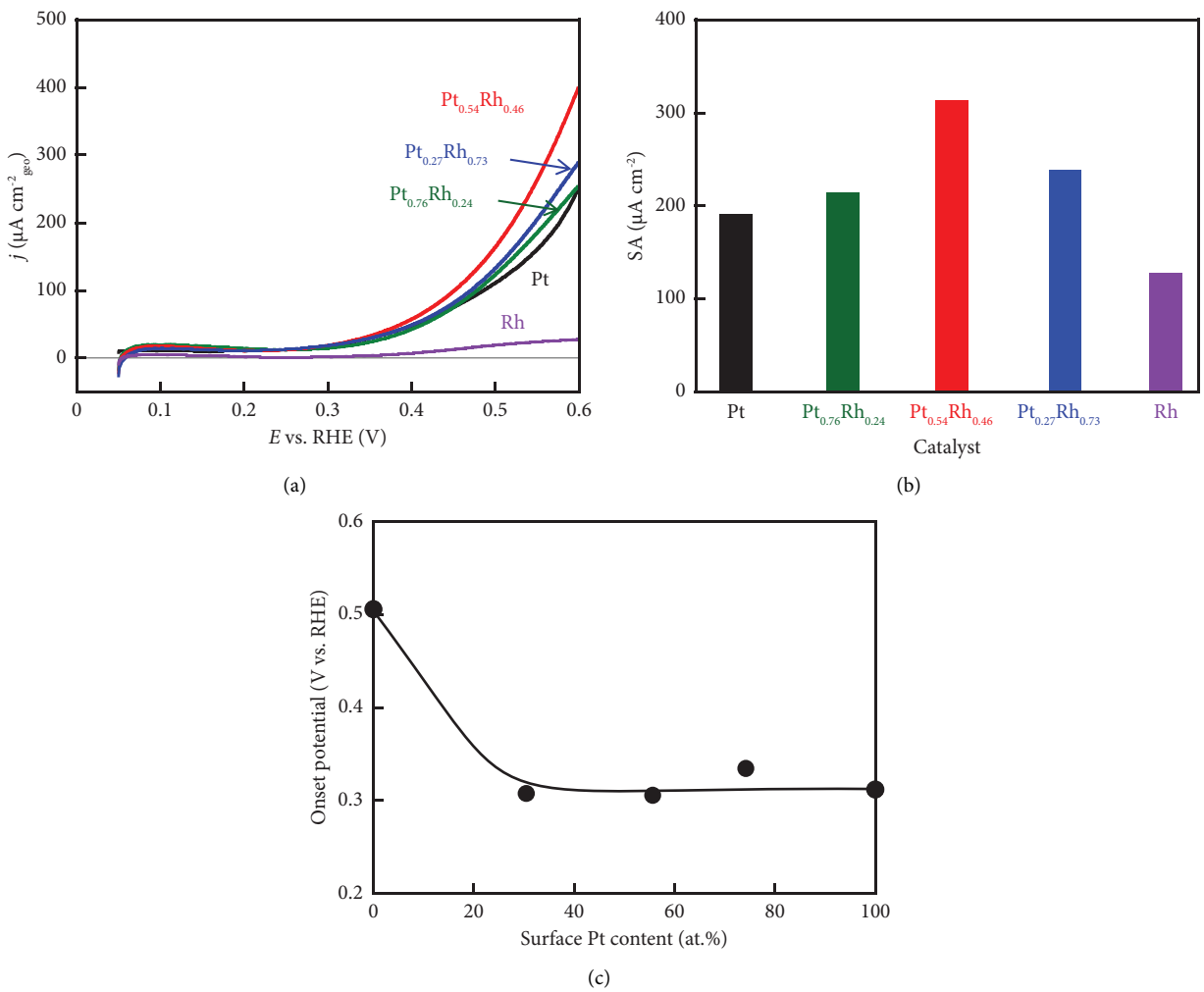

Figure 5: (a) EOR voltammograms and (b) SAs of Pt, Rh, $Pt_{0.76}Rh_{0.24}$, $Pt_{0.54}Rh_{0.46}$, and $Pt_{0.27}Rh_{0.73}$ solid solution electrodes. (c) Onset potentials of EOR as a function of Pt content estimated by XPS.

Figure 6 shows *in situ* IRAS spectra at various potentials in an Ar-saturated (1 M ethanol + 0.1 M $HClO_4$) solution for the Pt, Rh, $Pt_{0.76}Rh_{0.24}$, $Pt_{0.54}Rh_{0.46}$, and $Pt_{0.27}Rh_{0.73}$ solid solution electrodes. For the Pt electrode, the band around 2051 cm^{-1} assigned to linearly bonded CO (CO_L), which is a precursor of CO_2 formation, was observed at about 0.2 V, and the band intensity increased with potential, suggesting that the C-C bond was cleaved [38]. A band assigned to the asymmetric stretch vibration of CO_2 around 2343 cm^{-1} [39, 40] was not distinctly observed even at 0.6 V, suggesting that the oxidation of adsorbed CO does not occur. A band assigned to carbonyl around 1714 cm^{-1} due to the formation of acetaldehyde [41] appeared at 0.5 V. Therefore, the oxidation current observed at the Pt electrode (Figure 5(a)) is mainly attributed to the partial oxidation of ethanol to intermediates, not CO_2.

For the Rh electrode (Figure 6(b)), the bands assigned to linearly bonded CO (Rh-CO_L, 2016 cm^{-1}) and bridged CO on Rh (Rh-CO_B, 1900 cm^{-1}) [42] were observed around 0.2 V. The band assigned to carbonyl (1714 cm^{-1}) appeared at 0.5 V, whereas the band due to CO_2 (2343 cm^{-1}) was clearly observed at 0.6 V, as expected from the onset of CO-stripping on Rh at lower potentials (Figure 4(a)). This indicates that the CO_2 production on Rh occurs at lower potentials than that on Pt, but intermediates and/or CO_2 can poison the Rh surface, causing a significant decrease in EOR current (Figure 5(a)).

According to the EOR mechanism study [1], the EOR of the Pt_xRh_{1-x} ($x = 0.76$, 0.54, and 0.27) solid solutions are summarized in equations (2)–(8).

$$\mathrm{Pt} + \mathrm{CH_3CH_2OH} \longrightarrow \mathrm{Pt\text{–}CHOH\text{-}CH_{3ad}} + \mathrm{H^+} + \mathrm{e^-}, \quad (4)$$

$$\mathrm{Pt\text{–}CHOH\text{-}CH_{3ad}} \longrightarrow \mathrm{Pt\text{–}COH\text{-}CH_{3ad}} + \mathrm{H^+} + \mathrm{e^-}, \quad (5)$$

$$\mathrm{Pt\text{–}COH\text{-}CH_{3ad}} \longrightarrow \mathrm{Pt\text{–}CO\text{-}CH_{3ad}} + \mathrm{H^+} + \mathrm{e^-}, \quad (6)$$

$$\mathrm{Pt\text{–}CO\text{-}CH_{3ad}} + \mathrm{Rh} \longrightarrow \mathrm{Pt\text{–}CO\text{-}CH_{2ad}\text{–}Rh} + \mathrm{H^+} + \mathrm{e^-}, \quad (7)$$

$$\mathrm{Pt\text{–}CO\text{-}CH_{2ad}\text{–}Rh} \longrightarrow \mathrm{Pt\text{–}CO} + \mathrm{Rh\text{-}CH_{2ad}}. \quad (8)$$

Rh in Pt_xRh_{1-x} ($x = 0.76$, 0.54, 0.27) solid solution has two important functions. First, Rh can promote the cleavage of C-C bonds in EOR and inhibit the dehydrogenation

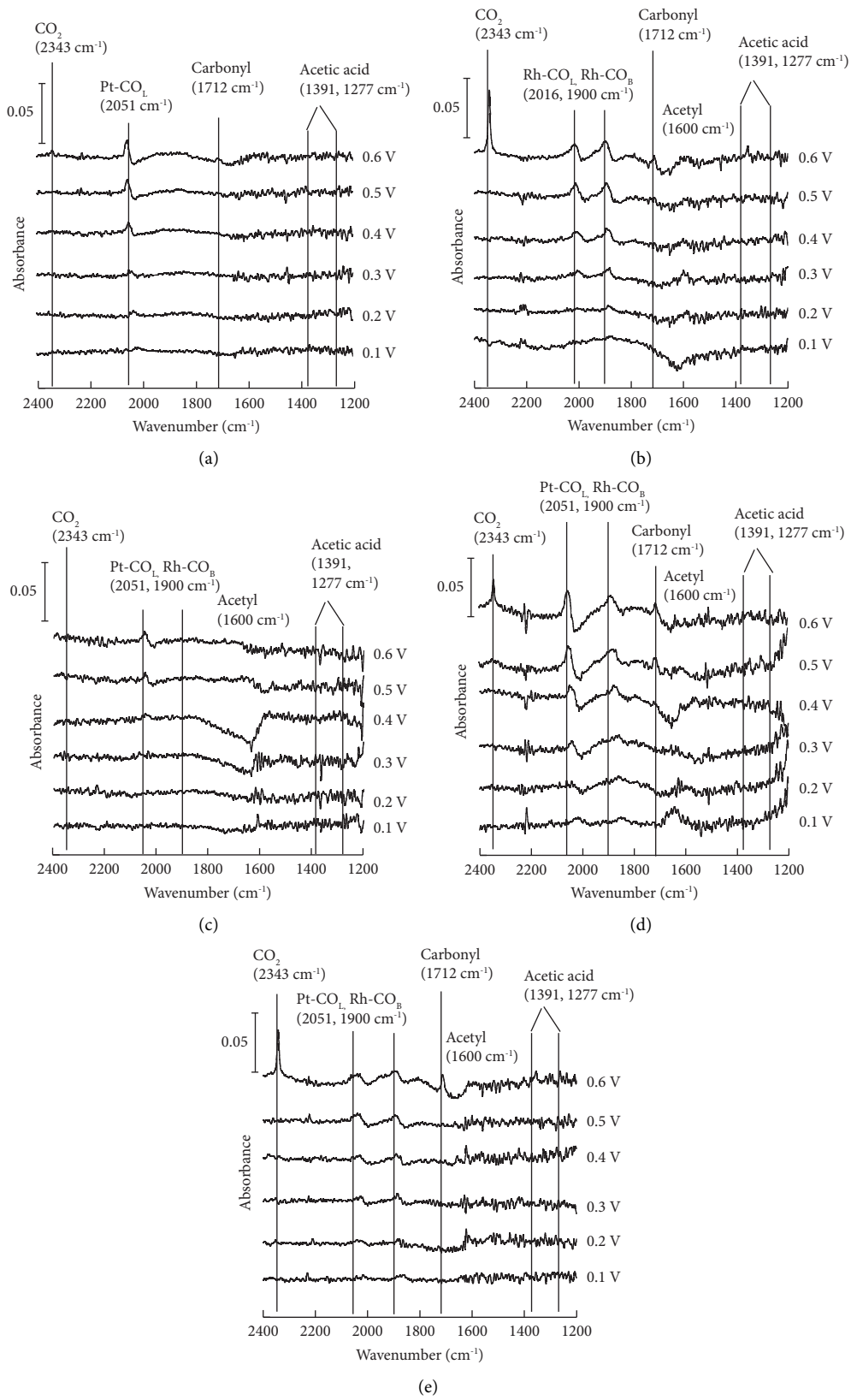

Figure 6: *In situ* IRAS spectra of (a) Pt, (b) Rh, (c) $Pt_{0.76}Rh_{0.24}$, (d) $Pt_{0.54}Rh_{0.46}$, and (e) $Pt_{0.27}Rh_{0.73}$ solid solution electrodes at various potentials.

process to form CH_3COOH and CH_3CHO. Second, Rh can provide the OH_{ads} species needed to oxidize intermediates such as CO adsorbed on adjacent Pt sites and avoid catalytic poisoning.

For the $Pt_{0.54}Rh_{0.46}$ solid solution electrode (Figure 6(d)), which had the highest SA in this study, the bands around 2051 cm^{-1} (Pt-CO_L) and 1900 cm^{-1} (Rh-CO_B) appeared around 0.2 V, whereas the band around 2016 cm^{-1} (Rh-CO_L) was not observed, suggesting that the C-C bond cleavage occurs at the adjacent Pt-Rh sites. The band around 1714 cm^{-1} due to carbonyl was observed around 0.4 V, and the band for CO_2 appeared at 2343 cm^{-1} was observed around 0.5 V, suggesting that EOR was accelerated due to the appearance of the Pt-Rh sites, as expected from Figure 5(a).

For the $Pt_{0.76}Rh_{0.24}$ solid solution electrode (Figure 6(c)), the band due to Pt-CO_L (2051 cm^{-1}) and the small shoulder around 2016 cm^{-1} due to Rh-CO_L appeared at 0.4 V, while the band for Rh-CO_B was not observed because the Rh sites were isolated surrounded by Pt sites, suggesting that the surface Pt and Rh atoms were uniformly arranged, as expected from Figure 1(b). Interestingly, similar to the Pt electrode, CO_2 and carbonyl were not detected even at 0.6 V. The oxidation of Rh-CO_L seems to be more difficult than that of Rh-CO_B, which is supported by the positive shift of E_{onset} of CO-stripping with increasing Pt content (Figure 4(c)). The EOR on the $Pt_{0.76}Rh_{0.24}$ solid solution electrode seems to mainly occur at Pt sites modified electronically by alloying with Rh, improving the EOR activity.

For the Rh-rich $Pt_{0.27}Rh_{0.73}$ solid solution electrode (Figure 6(e)), the bands due to Rh-CO_B (1900 cm^{-1}) and Rh-CO_L (2016 cm^{-1}) appeared around 0.2 V, while the small band due to Pt-CO_L was also observed as a shoulder around 0.4 V because the Pt sites were isolated surrounded by Rh sites. The bands due to carbonyl (1714 cm^{-1}) and CO_2 (2343 cm^{-1}) were observed around 0.4 V, and the strong band for CO_2 appeared at 0.6 V, similar to the Rh electrode. The $Pt_{0.27}Rh_{0.73}$ solid solution has the fewer adjacent Pt-Rh sites than $Pt_{0.54}Rh_{0.46}$, reducing the C-C bond cleavage at the Pt-Rh sites. The appearance of Rh-CO_L may be responsible of the delayed CO_2 production.

4. Conclusions

We prepared Pt_xRh_{1-x} ($x = 0.76$, 0.54, and 0.27) solid solutions by the arc-melting method. Their lattice constant and bulk composition followed the Vegard equation. For each solid solution, the surface composition estimated by XPS was quite similar to the bulk composition estimated by EDX. The CO-stripping voltammograms demonstrated that the E_{onset} value of CO oxidation shifted negatively as the Pt content in the solid solutions decreased, which indicated an enhancement of CO-poisoning resistance for the solid solutions with lower Pt contents. From the LSV analysis of each solid solution electrode in an Ar-saturated (1 M ethanol + 0.1 M $HClO_4$) solution, it was found that the $Pt_{0.54}Rh_{0.46}$ electrode gave the highest specific activity of 312 $\mu A \cdot cm^{-2}$, which was about 1.8 and 2.5 times higher than the SAs of the Pt and Rh electrodes, respectively. From the *in situ* IRAS analysis, no band of CO_2 was observed even at 0.6 V for Pt and $Pt_{0.76}Rh_{0.24}$ electrodes, but band of CO_2 was clearly observed at 0.5 or 0.6 V for Rh, $Pt_{0.27}Rh_{0.73}$, and $Pt_{0.54}Rh_{0.46}$ electrodes. In addition, the *in situ* IRAS clearly illustrated the increase of a peak at 2343 cm^{-1} assigned to CO_2 at potentials above 0.5 V for the $Pt_{0.54}Rh_{0.46}$ solid solution electrode, suggesting the EOR activity of the $Pt_{0.54}Rh_{0.46}$ electrode was higher than that of $Pt_{0.76}Rh_{0.24}$ and $Pt_{0.27}Rh_{0.73}$ electrodes.

Data Availability

The data used to support the findings of this study are available from the corresponding author upon reasonable request.

Conflicts of Interest

The authors declare that they have no conflicts of interest regarding the publication of this paper.

Acknowledgments

This research was supported by the research funds provided by Osaka Metropolitan University.

References

[1] Y. Zhu, L. Bu, Q. Shao, and X. Huang, "Subnanometer PtRh nanowire with alleviated poisoning effect and enhanced C–C bond cleavage for ethanol oxidation electrocatalysis," *ACS Catalysis*, vol. 9, no. 8, pp. 6607–6612, 2019.

[2] J. Ribeiro, D. M. dos Anjos, K. B. Kokoh et al., "Carbon-supported ternary PtSnIr catalysts for direct ethanol fuel cell," *Electrochimica Acta*, vol. 52, no. 24, pp. 6997–7006, 2007.

[3] M. Z. F. Kamarudin, S. K. Kamarudin, M. S. Masdar, and W. R. W. Daud, "Review: direct ethanol fuel cells," *International Journal of Hydrogen Energy*, vol. 38, no. 22, pp. 9438–9453, 2013.

[4] S. P. S. Badwal, S. Giddey, A. Kulkarni, J. Goel, and S. Basu, "Direct ethanol fuel cells for transport and stationary applications – a comprehensive review," *Applied Energy*, vol. 145, pp. 80–103, 2015.

[5] J. P. I. de Souza, S. L. Queiroz, K. Bergamaski, E. R. Gonzalez, and F. C. Nart, "Electro-oxidation of ethanol on Pt, Rh, and PtRh electrodes. A study using DEMS and in-situ FTIR techniques," *The Journal of Physical Chemistry B*, vol. 106, no. 38, pp. 9825–9830, 2002.

[6] R. Kavanagh, X.-M. Cao, W.-F. Lin, C. Hardacre, and P. Hu, "Origin of low CO_2 selectivity on Platinum in the direct ethanol fuel cell," *Angewandte Chemie International Edition*, vol. 51, no. 7, pp. 1572–1575, 2012.

[7] H.-F. Wang and Z.-P. Liu, "Comprehensive mechanism and structure-sensitivity of ethanol oxidation on Platinum: new transition-state searching method for resolving the complex reaction network," *Journal of the American Chemical Society*, vol. 130, no. 33, pp. 10996–11004, 2008.

[8] H. A. Asiri and A. B. Anderson, "Mechanisms for ethanol electrooxidation on Pt(111) and adsorption bond strengths defining an ideal catalyst," *Journal of the Electrochemical Society*, vol. 162, no. 1, pp. 115–122, 2015.

[9] F. Zhu, K. Tu, L. Huang et al., "High selectivity PtRh/RGO catalysts for ethanol electro-oxidation at low potentials:

enhancing the efficiency of CO_2 from alcoholic groups," *Electrochimica Acta*, vol. 292, pp. 208–216, 2018.

[10] J. Bai, X. Xiao, Y.-Y. Xue et al., "Bimetallic platinum–rhodium alloy nanodendrites as highly active electrocatalyst for the ethanol oxidation reaction," *ACS Applied Materials & Interfaces*, vol. 10, no. 23, pp. 19755–19763, 2018.

[11] M. H. Shao and R. R. Adzic, "Electrooxidation of ethanol on a Pt electrode in acid solutions: in situ ATR-SEIRAS study," *Electrochimica Acta*, vol. 50, no. 12, pp. 2415–2422, 2005.

[12] C. Lamy, S. Rousseau, E. M. Belgsir, C. Coutanceau, and J. M. Leger, "Recent progress in the direct ethanol fuel cell: development of new platinum–tin electrocatalysts," *Electrochimica Acta*, vol. 49, no. 22-23, pp. 3901–3908, 2004.

[13] L. Jiang, L. Colmenares, Z. Jusys, G. Q. Sun, and R. J. Behm, "Ethanol electrooxidation on novel carbon supported Pt/SnOx/C catalysts with varied Pt:Sn ratio," *Electrochimica Acta*, vol. 53, no. 2, pp. 377–389, 2007.

[14] E. Higuchi, T. Takase, M. Chiku, and H. Inoue, "Preparation of ternary Pt/Rh/SnO_2 anode catalysts for use in direct ethanol fuel cells and their electrocatalytic activity for ethanol oxidation reaction," *Journal of Power Sources*, vol. 263, pp. 280–287, 2014.

[15] V. M. Schmidt, R. Ianniello, E. Pastor, and S. González, "Electrochemical reactivity of ethanol on porous Pt and PtRu: oxidation/reduction reactions in 1 M $HClO_4$," *Journal of Physical Chemistry*, vol. 100, no. 45, pp. 17901–17908, 1996.

[16] G. Camara, R. B. de Lima, and T. Iwasita, "Catalysis of ethanol electrooxidation by PtRu: the influence of catalyst composition," *Electrochemistry Communications*, vol. 6, no. 8, pp. 812–815, 2004.

[17] R. Rizo, D. Sebastian, M. J. Lazaro, and E. Pastor, "On the design of Pt-Sn efficient catalyst for carbon monoxide and ethanol oxidation in acid and alkaline media," *Applied Catalysis B: Environmental*, vol. 200, pp. 246–254, 2017.

[18] A. Kowal, S. Gojković, K.-S. Lee, P. Olszewski, and Y.-E. Sung, "Synthesis, characterization and electrocatalytic activity for ethanol oxidation of carbon supported Pt, Pt–Rh, Pt–SnO_2 and Pt–Rh–SnO_2 nanoclusters," *Electrochemistry Communications*, vol. 11, no. 4, pp. 724–727, 2009.

[19] E. Higuchi, K. Miyata, T. Takase, and H. Inoue, "Ethanol oxidation reaction activity of highly dispersed Pt/SnO_2 double nanoparticles on carbon black," *Journal of Power Sources*, vol. 196, no. 4, pp. 1730–1737, 2011.

[20] H. Wang, X. Tong, S. Sun, and M. Mohamedi, "Nanostructured shrub-like bimetallic Pt_xRh_{100-x} alloys grown on carbon paper for the oxidative removal of adsorbed carbon monoxide for ethanol fuel cells reaction," *Electrochimica Acta*, vol. 355, Article ID 136823, 2020.

[21] P. Wang, S. Yin, Y. Wen et al., "Ternary Pt_9RhFe_x nanoscale alloys as highly efficient catalysts with enhanced activity and excellent CO-poisoning tolerance for ethanol oxidation," *ACS Applied Materials & Interfaces*, vol. 9, no. 11, pp. 9584–9591, 2017.

[22] F. Alcaide, G. Álvarez, P. L. Cabot et al., "Supporting PtRh alloy nanoparticle catalysts by electrodeposition on carbon paper for the ethanol electrooxidation in acidic medium," *Journal Of Electroanalytical Chemistry*, vol. 861, Article ID 113960, 2020.

[23] R. M. C. Silva, G. A. Camara, and M. J. Giz, "Electro-oxidation of ethanol on PtRh surfaces partially covered by Sn," *Electrochimica Acta*, vol. 308, pp. 167–173, 2019.

[24] A. B. Delpeuch, T. Asset, M. Chatenet, and C. Cremers, "Electrooxidation of ethanol at room temperature on carbon-supported Pt and Rh-containing catalysts: a DEMS study," *Journal of the Electrochemical Society*, vol. 161, no. 9, pp. F918–F924, 2014.

[25] D. A. Cantane, W. F. Ambrosio, M. Chatenet, and F. H. B. Lima, "Electro-oxidation of ethanol on Pt/C, Rh/C, and Pt/Rh/C-based electrocatalysts investigated by on-line DEMS," *Journal of Electroanalytical Chemistry*, vol. 681, pp. 56–65, 2012.

[26] J. Piwowar and A. Lewera, "On the absence of a beneficial role of Rh towards C–C bond cleavage during low temperature ethanol electrooxidation on PtRh nanoalloys," *Journal of Electroanalytical Chemistry*, vol. 875, Article ID 114229, 2020.

[27] L. Fang, F. J. Vidal-Iglesias, S. E. Huxter, G. A. Attard, and P. B. Wells, "RhPt/graphite catalysts for CO electrooxidation: performance of mixed metal and alloyed surfaces," *Surface Science*, vol. 631, pp. 258–266, 2015.

[28] A. Karschin, I. Katsounaros, S. O. Klemm, J. C. Meier, and K. J. J. Mayrhofer, "Degradation of polycrystalline rhodium and rhodium nanoparticles," *Electrochimica Acta*, vol. 70, pp. 355–359, 2012.

[29] D. A. J. Rand and R. Woods, "Determination of the surface composition of smooth noble metal alloys by cyclic voltammetry," *Journal of Electroanalytical Chemistry and Interfacial Electrochemistry*, vol. 36, no. 1, pp. 57–69, 1972.

[30] T. Biegler, D. A. J. Rand, and R. Woods, "Limiting oxygen coverage on platinized platinum; Relevance to determination of real platinum area by hydrogen adsorption," *Journal of Electroanalytical Chemistry and Interfacial Electrochemistry*, vol. 29, no. 2, pp. 269–277, 1971.

[31] M. Łukaszewski, M. Soszko, and A. Czerwiński, "Electrochemical methods of real surface area determination of noble metal electrodes – an Overview," *International Journal Of Electrochemical Science*, vol. 11, no. 6, pp. 4442–4469, 2016.

[32] J. Nash, X. Yang, J. Anibal, J. Wang, Y. Yan, and B. Xu, "Electrochemical nitrogen reduction reaction on noble metal catalysts in proton and hydroxide exchange membrane electrolyzers," *Journal of the Electrochemical Society*, vol. 164, no. 14, pp. F1712–F1716, 2017.

[33] W. Tokarz, H. Siwek, P. Piela, and A. Czerwiński, "Electrooxidation of methanol on Pt-Rh alloys," *Electrochimica Acta*, vol. 52, no. 18, pp. 5565–5573, 2007.

[34] B. Hammer, Y. Morikawa, and J. K. Nørskov, "CO chemisorption at metal surfaces and overlayers," *Physical Review Letters*, vol. 76, no. 12, pp. 2141–2144, 1996.

[35] Y. Liu, L. Du, F. Kong et al., "Sulfur dioxide-tolerant bimetallic PtRu catalyst toward oxygen electroreduction," *ACS Sustainable Chemistry & Engineering*, vol. 8, no. 2, pp. 1295–1301, 2020.

[36] M. Wakisaka, S. Mitsui, Y. Hirose, K. Kawashima, H. Uchida, and M. Watanabe, "Electronic structures of Pt-Co and Pt-Ru alloys for CO-tolerant anode catalysts in polymer electrolyte fuel cells studied by EC-XPS," *The Journal of Physical Chemistry B*, vol. 110, no. 46, pp. 23489–23496, 2006.

[37] D. Donadio, L. M. Ghiringhelli, and L. Delle Site, "Autocatalytic and cooperatively stabilized dissociation of water on a stepped platinum surface," *Journal of the American Chemical Society*, vol. 134, no. 46, pp. 19217–19222, 2012.

[38] H. Wang and H. D. Abruña, "Adsorbed enolate as the precursor for the C–C bond splitting during ethanol electrooxidation on Pt," *Journal of the American Chemical Society*, vol. 145, no. 11, pp. 6330–6338, 2023.

[39] M. Li, A. Kowal, K. Sasaki et al., "Ethanol oxidation on the ternary Pt–Rh–SnO_2/C electrocatalysts with varied Pt–Rh–Sn ratios," *Electrochimica Acta*, vol. 55, no. 14, pp. 4331–4338, 2010.

[40] N. Erini, R. Loukrakpam, V. Petkov et al., "Ethanol electro-oxidation on ternary platinum–rhodium–tin nanocatalysts: insights in the atomic 3D structure of the active catalytic phase," *ACS Catalysis*, vol. 4, no. 6, pp. 1859–1867, 2014.

[41] J. Torrero, M. A. Peña, M. Retuerto, L. Pascual, and S. Rojas, "Infrared study of the electrooxidation of ethanol in alkaline electrolyte with Pt/C, PtRu/C and Pt_3Sn," *Electrochimica Acta*, vol. 319, pp. 312–322, 2019.

[42] F. Vigier, C. Coutanceau, F. Hahn, E. M. Belgsir, and C. Lamy, "On the mechanism of ethanol electro-oxidation on Pt and PtSn catalysts: electrochemical and in situ IR reflectance spectroscopy studies," *Journal of Electroanalytical Chemistry*, vol. 563, no. 1, pp. 81–89, 2004.